SUBSTRATE BARRIER EFFECTS ON TOTAL HEAT TRANSFER FOR A R-30 FIBROUS INSULATION BATT

K.T. Harris[+], J.A. Roux[#], T.A. McCarty*
Department of Mechanical Engineering
University of Mississippi
University, MS 38677

ABSTRACT

By implementing various substrate barriers to a R-30 fiberglass insulation batt, this research shows the overall changes in the substrate heat flux. Independently, a plastic vapor barrier, and both a perforated and non-perforated radiant barriers are analyzed in this study. Conduction, radiation heat transfer and moisture (mass) transport are considered to be the main contributors to heat transport within attic fiberglass insulation. A transient, one-dimensional, computational thermal model has been developed to simultaneously model all three of these heat transport mechanisms, which allows the total heat flux at the attic insulation substrate to be predicted. This numerical model has the capabilities to determine the effect on each of the three modes of heat transfer once a substrate barrier has been added. Summertime experimental data were collected at an occupied North Mississippi residence for cases with and without a vapor barrier at the substrate for R-30 fiberglass insulation. Within this investigation experimental and predicted total heat transfer results are compared and analyzed. Profiles such as temperature-time histories, vapor H_2O concentrations, and individual modes of heat transfer plots are presented to support the experimentally determined overall effects on the heat transfer at the substrate once a substrate barrier has been implemented.

[+]Graduate Student; [#]Professor; [*]Assistant Professor

NOMENCLATURE

		Units
c_f	Specific heat of fiberglass	J/kg-K
h_{ad}	Heat of absorption/desorption	
I	Radiative intensity	W/m^2
i_b	Specific enthalpy of liquid	
i_v	Specific enthalpy of vapor	
k_f	Thermal conductivity of fiberglass	W/m-K
m_b	Mass concentration of bound H_2O	kg bound H_2O/m^3
m_v	Mass concentration of vapor H_2O	kg vapor H_2O/m^3
$\dot{m}_b$	Rate of absorption of bound H_2O (= $-\dot{m}_v$)	sec^{-1}
m_ϕ	Constant in Equation (3a), Table 1	
n	Refractive index of medium	
q_T	Total heat flux, Eqs.(7a&7b)	W/m^2
q_r	Radiative heat flux	W/m^2
$\dot{q}$	Volumetric heat source/sink, Eq.(4a)	W/m^3
T	Temperature	K
T_a	Attic temperature	K
T_c	Ceiling temperature	K
T_o	Top of batt temperature	K
T_r	Roof temperature	K
T_R	Reference temperature	K
T_s	Substrate temperature	K
t	Time	sec
X	Mass of absorbed moisture/mass of fiberglass	kg H_2O/kg dry fbgls
y	Physical thickness	cm
y_o	Total thickness	cm
Greek		
β	Extinction coefficient	cm^{-1}
ϵ_r	Emissivity of the roof	

ϵ_s	Emissivity of the substrate	
γ_b	Diffusion coefficient of liquid	m^2/sec
γ_v	Diffusion coefficient of vapor	m^2/sec
μ	Cosine of polar angle	
ϕ	Relative humidity	
Ψ	Azmuthial Angle	degrees
θ	Polar angle	degrees
ρ_f	Density of fiberglass	kg/m^3
ρ_r	Reflectivity of the roof	
ρ_s	Reflectivity of the substrate	
τ	Local optical depth (βy)	
τ_o	Total optical depth (βy_o)	
ω	Single scatter albedo	

Subscripts

b	Bound
B	Radiant blackbody
f	Fiberglass
o	Top surface
r	Roof
R	Reference
s	Substrate
v	Vapor

INTRODUCTION

This investigation is a companion paper to Ref. [1] which investigated the effects of a substrate barrier for R-19 insulation. The R-19 investigation yielded some significant findings; the time-integrated heat transfer at the substrate was reduced by 13% when a plastic non-perforated vapor barrier was added to the substrate (bottom of batt) when compared to a no vapor barrier case. This work will focus on similar issues (moisture has been found, in previous works [2-5], to increase the heat transfer through fiberglass attic insulation and into the living spaces of a home

under humid summer conditions) for R-30 insulation. Once again through a thorough literature survey and several personal contacts [6-8] it has been determined that there is knowledge of the fact that moisture is instrumental in increasing the substrate heat transfer but there has been no work found to determine (quantify) the impact on heat transfer of adding a plastic vapor barrier to the substrate as compared to a no vapor barrier situation other than the above mentioned R-19 investigation [1]. This study shows the effect that a plastic vapor barrier substrate has on the overall heat transfer through a R-30 fiberglass insulation batt. Experimental data with and without the plastic vapor barrier were collected and compared to the results of an analytical/numerical model. The numerical/analytical model was used to help explain the coupling of the three modes of heat transfer (conduction, radiation heat transfer and moisture transport) and how these coupled modes are affected by the application of various substrate barriers between the attic insulation batt and the ceiling gypsum board.

The implementation of a foil radiant barrier at the top of the insulation batt has been studied in previous works [4-5]. In this study, as in its companion work [1], a theoretical investigation of adding a non-perforated foil radiant barrier and a perforated foil radiant barrier at the substrate of the insulation batt was performed. The substrate heat flux in Ref. [1] was not reduced significantly when a foil radiant barrier was added to the substrate (less than 1% reduction). Excluding the R-19 insulation paper [1], no work has been found quantifying the effect of employing a radiant "substrate" barrier for either R-19 or R-30 insulations.

This investigation will further go on and look at the combination of having both a radiant foil barrier at the top of the batt and a plastic vapor barrier at the bottom of the fiberglass insulation batt. Reference [1] investigated this combination for a R-19 fiberglass batt and found significant reductions in the substrate heat flux ($\approx$ 53% reduction). This paper will determine

whether or not the same magnitude of reduction can be achieved for R-30 for such a combination of radiant and vapor barriers. The analytical/numerical model was used to illustrate how the different modes of heat transfer are affected and/or altered by the addition of a foil radiant substrate barrier. Will the individual modes of heat transfer be impacted or will the substrate heat transfer increase or decrease with the application of a substrate barrier are two of the questions which will be answered in this study. Experimental temperature and relative humidity data obtained for the plastic vapor barrier case were used as the input parameters in the numerical/analytical model for the non-perforated foil radiant barrier substrate simulation and temperature and relative humidity data obtained from the no plastic vapor barrier case were used as the input parameters for simulating the perforated radiant barrier substrate case.

EXPERIMENTAL SETUP

Shown in Fig. 1 is the attic geometry for the experimental setup corresponding to the North Mississippi residence where data were collected. The insulation top boundary is the attic air and the substrate boundary is gypsum board for the cases without a vapor or radiant barrier at the bottom of the insulation. Experimental data were recorded for the case of a plastic (polyethylene - .0024 cm) vapor barrier, but only predictions were made for the case of a radiant substrate barrier. Also it should be noted that the coordinate system originates at the substrate where $y=0$ and hence at the top of the insulation batt $y=y_o$.

Data were collected for a horizontally oriented R-30 fiberglass insulation batt. All experimental data were recorded every 15 minutes using an HP 3528A data acquisition system. All data channels were sampled 100 times at each 15 minute data acquisition interval in order to improve the signal/noise ratio. Temperatures (see Fig. 2) were measured with type-J thermocouples. Relative humidities were measured with Hycal CT-829-A-RX temperature

compensated relative humidity (R.H.) meters (see Fig. 2) that are accurate to less than 1% between 20<R.H.<80%. Heat fluxes were measured with the Hycal BI-7-20-WP-J-X-X6 high sensitivity heat flux meters (see Fig. 2); the heat flux meters (5.1 cm square by 3mm thick) were calibrated by Holometrix Inc. and are stated to be accurate to $\pm$5% of full scale (heat flux of 7.8 W/m^2). Heat flux data were taken for the top and substrate surface fluxes however the top surface heat flux measurements were only used to validate the numerical model. At the substrate the heat flux meters were located at the interface between the fiberglass batt and gypsum board; when a vapor barrier was employed at the substrate, a heat flux meter was placed between the fiberglass and vapor barrier and another heat flux meter was placed between the vapor barrier and the gypsum board allowing the two heat flux meters to be in parallel of one another. For all cases these two heat flux meters showed excellent agreement (less than 3% difference).

NUMERICAL/ANALYTICAL MODEL

The numerical/analytical model described in this section has been utilized as an analysis tool in previous studies by the authors including Refs. [4,5]. It is outlined again in this paper for the purpose of clarity and continuity. The basic equations for the numerical/analytical model are the species equations, the energy equation, and the radiative transport equation. To simplify the model, the attic insulation is considered to behave like a plane parallel layer and the primary assumptions are given as follows: 1) transient, one-dimensional combined conduction, radiation heat transfer with mass (H_2O) diffusion, and absorption/desorption of H_2O; 2) volumetric radiation within the fiberglass insulation which was considered as an absorbing, emitting and scattering (isotropic) medium; 3) gray radiative properties (extinction coefficient and albedo); 4) convection is neglected within the insulation batt however convection at the top surface of the batt is implicitly included in the measured top surface (T_o) temperature ; 5) relative humidities and

temperatures at the boundaries are known (measured) functions of time.

This work also considers the heat of H_2O absorption to be equal to the heat of$_2$H O desorption and it neglects the small hystersis phenomenon present between the absorption and desorption isotherms. The density of the fiberglass insulation was assumed to be the same as the referenced density of 12 kg/m^3 [9]. The temperatures at the insulation top, bottom, and roof are the required boundary condition information for solving the energy equation and the radiative transport equation. The boundary temperatures and relative humidities are required for obtaining concentrations of bound H_2O and vapor H_2O species which are needed for solving the species equations. Emissivities are specified at the roof ($\epsilon_r=1-\rho_r=.85$) and substrate ($\epsilon_s=1-\rho_s=.95$) for the no barrier and plastic vapor barrier surfaces and ($\epsilon_s=1-\rho_s=.05$) for the radiant barrier cases [10]. That thermal/radiative properties used in this model are presented in Table 1.

Solution Scheme

The basic equations were solved simultaneously by an iterative scheme that employs a control volume based finite difference method (Patankar [11]). The transient solution is obtained by marching forward in time with an appropriate time step (5 min time step). A time step that yielded no change in the converged temperatures and species concentrations was considered an appropriate time step. A non-uniform spatial grid with 33 nodal points was used to achieve lower computational time without sacrificing accuracy; the computation time on an IBM 3084 to predict all the results for a 24 hour period was about 30 seconds of CPU time. It should be noted that the experimental data were recorded every 15 minutes and hence a linear interpolation was used to input boundary condition information within the numerical model at the 5 minutes time step intervals which occur in between the 15 minute data acquisition intervals for the experimental data. The convergence criteria at each time step for temperature was .001 C and for H_2O species

concentration was 1%. The average number of iterations to achieve convergence at each time step was 95.

Species Equations

For one-dimensional unsteady moisture transport, the species equation for bound H_2O (where bound means H_2O which exists within the phenolic binder) can be expressed as

$$\frac{\partial m_b}{\partial t} - \frac{\partial}{\partial y}\left(\gamma_b \frac{\partial m_b}{\partial y}\right) = \dot{m}_b \qquad (1)$$

Here, $\dot{m}_b$ is the rate of absorption/desorption of bound H_2O (sink/source term). Similarly, the species conservation equation for vapor H_2O can be written as

$$\frac{\partial m_v}{\partial t} - \frac{\partial}{\partial y}\left(\gamma_v \frac{\partial m_v}{\partial y}\right) = \dot{m}_v \qquad (2)$$

In Eq. (2), all the terms are similar to those in Eq. (1) except that the subscript "v" denotes vapor H_2O. The source terms ($\dot{m}_b$,$\dot{m}_v$) in Eqs. (1) and (2) account for H_2O absorption/desorption. The H_2O mass sorption isotherms are given in Ref. [12]. Since the heat of absorption and desorption for the phenolic binder are not readily available, it is considered that the binder's heat of absorption and desorption acts as zeolite whose properties for H_2O are known [13,14]. It should be noted that the rate of absorption of bound H_2O is equal to rate of desorption of vapor H_2O and vice versa. Therefore, the source terms are given by

$$\dot{m}_b = - \dot{m}_v = \rho_f \frac{\partial X}{\partial t} \qquad (3)$$

where

$$\frac{\partial X}{\partial t} = m_\phi \frac{\partial \phi}{\partial t} \tag{3a}$$

In Eq. (3a), m_ϕ is a constant obtained from the data presented in Ref. [12] and is given in Table 1. The symbol ϕ is the relative humidity and Eqs. (3) and (3a) yield the moisture mass absorption/desorption as a function of the relative humidity in accordance with Ref. [15] which reported the absorption isotherm to be a function of relative humidity only and not a separate function of temperature. The quantity X is dimensionless and has units of kg H_2O/kg dry fiberglass.

The boundary conditions for Eqs. (1) and (2) are given by

$$m_b = (m_b)_s(t); \quad m_v = (m_v)_s(t) \quad \text{at} \quad y = 0$$

$$m_b = (m_b)_o(t); \quad m_v = (m_v)_o(t) \quad \text{at} \quad y = y_o$$

where these concentrations were determined from the measured relative humidity and dry-bulb temperature at the bottom and top of the insulation batt. Linear vapor and bound H_2O concentration profiles were chosen as the initial concentration conditions (midnight, t=0).

Energy Equation

The one-dimensional energy equation for transient, coupled conduction, radiation heat transport, diffusion of vapor H_2O and bound H_2O, and absorption/desorption of H_2O is given by

$$\frac{\partial}{\partial y}\left(k_f \frac{\partial T}{\partial y}\right) - \frac{\partial q_r}{\partial y} + \frac{\partial}{\partial y}\left(\gamma_v i_v \frac{\partial m_v}{\partial y}\right) + \frac{\partial}{\partial y}\left(\gamma_b i_b \frac{\partial m_b}{\partial y}\right) + \dot{q} = \rho_f c_f \frac{\partial T}{\partial t} \tag{4}$$

where

$$\dot{q} = h_{ad} \dot{m}_b$$

with boundary conditions:

$$T = T_s(t) \text{ at } y = 0$$

$$T = T_o(t) \text{ at } y = y_o$$

where $T_s(t)$ and $T_o(t)$ are the measured temperatures at the bottom and the top of the insulation batt, respectively. A linear temperature profile was chosen as the initial temperature condition (midnight, $t = 0$). The terms on the left hand side of the Eq. (4) represent heat conduction, volumetric radiation, diffusion of vapor H_2O and bound H_2O, and the heat source/sink due to H_2O absorption/ desorption within the insulation binder respectively, whereas the term on the right hand side is the transient term.

Radiative Transport Equation

The radiative heat flux, q_r, is required for solving the energy equation, Eq. (4); it is obtained by solving the radiative transport equation as presented below. The one-dimensional axially symmetric radiative transport equation for an absorbing, emitting, and isotopically scattering medium from Ref. [16] can be written as

$$\mu \frac{dI(\tau,\mu)}{d\tau} = -I(\tau,\mu) + \frac{\omega}{2}\int_{-1}^{1} I(\tau,\mu')\, d\mu' + n^2(1-\omega)\, I_b(T(\tau)) \qquad (5)$$

The boundary conditions for Eq. (5) are given by

$$I(0,\mu) = \rho_s I(0,-\mu) + (1-\rho_s)n^2 I_B(T_s), \qquad \mu > 0$$
$$I(\tau_o,-\mu) = \rho_r I(\tau_o,+\mu) + (1-\rho_r)r^2 I_B(T_r), \quad \mu > 0$$

where $I_B(T_r) = e_B(T_r)/\pi$ and for a gray-body material $e_B(T_r) = \sigma T_r^4$. Here, ρ_s is the reflectivity of the substrate and ρ_r is the reflectivity of the roof for the no foil above the insulation case. If a foil

radiant barrier is used above the insulation, then ρ_n is the reflectance (.95) of the foil and T_r is then equal to the top of the batt temperature T_o. It should be noted that n=1 for this problem. A quasi-analytical technique with the method of discrete ordinates, employing a 16 point Gaussian quadrature, was used in solving the radiative transport equation (Eq. (5)) and the details are documented in Refs. [16,17]. The radiative heat flux needed in Eq. (4) is given by definition as

$$q_r(\tau) = \int_0^{2\Pi} \int_{-1}^{1} I(\tau,\mu)\mu d\mu d\psi \qquad (6)$$

The total heat flux for the no plastic vapor barrier case or the perforated radiant substrate barrier case is given by the following

$$q_T = -k_f \frac{\partial T}{\partial y}\Big)_{y=0} + q_r(0) - \gamma_v \frac{\partial m_v}{\partial y} i_v\Big)_{y=0} - \gamma_b \frac{\partial m_b}{\partial y} i_b\Big)_{y=0} \qquad (7a)$$

where the first term on the right is the conduction term, the second is the radiation term, the third is the diffused H_2O vapor term, and the fourth is the diffused bound H_2O term. It was assumed that the perforated radiant barrier substrate did not retard the diffusion of vapor H_2O through the barrier in any way. Equation (7b) below is used for the total heat flux when a plastic or non-perforated radiant vapor barrier is implemented at the substrate

$$q_T = -k_f \frac{\partial T}{\partial y}\Big)_{y=0} + q_r(0) - \gamma_v \frac{\partial m_v}{\partial y} h_{ad}\Big)_{y=0} \qquad (7b)$$

It can be seen that Eqs. (7a) and (7b) are similar in that they both have the conduction and radiation terms but differ in that once a vapor (plastic or non-perforated radiant) barrier is in

place the vapor cannot diffuse through the substrate/fiberglass interface, hence the H_2O mass transfer term in Eq. (7b) represents the mass flow (absorbed/desorbed) into or out of the phenolic binder at the bottom of the batt.

RESULTS

The results of this investigation will focus on the effects of adding a substrate barrier (non-perforated plastic vapor barrier or non-perforated foil radiant barrier or perforated foil radiant barrier) to a R-30 fiberglass insulation batt on the total heat flux through the insulation batts. There is a companion paper [1] that investigated the effects on R-19 insulation batts. For R-19 it was discovered that a plastic vapor barrier reduced the integrated heat flux (during the heating portion of the day) by 13% when compared to a non-barrier case (standard R-19 batt). It was also found that perforated and non-perforated foil radiant barrier substrates had an insignificant effect on the heat flux through the insulation batt when compared to a R-19 standard (no substrate) batt and a plastic vapor barrier substrate batt, respectively. The results for R-30 insulation are divided into three sections; plastic vapor barrier substrate only, foil radiant barrier substrate only, and the combination of a plastic vapor barrier at the bottom (substrate) of the batt and a perforated foil radiant barrier at the top of the batt. Experimental data are presented for the case of a plastic vapor barrier and the combination case mentioned in the previous sentence.

The results for batts with a perforated and non-perforated foil radiant barrier at the substrate are predictions. No experimental data were obtained for these two cases. The non-perforated foil radiant barrier was considered to act as a plastic vapor barrier except that in the numerical/analytical model the reflectance at the substrate was changed from gypsum board (ρ_s= .05) to that of aluminum foil (ρ_s= .95). The temperature and relative humidity data were assumed to be the same as that measured for the plastic vapor barrier case. Likewise the

perforated foil radiant barrier substrate was simulated in the numerical/analytical model by the temperature and relative humidity data for a batt with no barrier at the substrate (standard R-30 batt) and again the reflectance was changed from that of gypsum board to aluminum foil.

Plastic Vapor Barrier

The following results are for typical Northern Mississippi summer conditions. Figure 3 displays the temperature-time histories for a R-30 fiberglass insulation batt with a plastic vapor barrier at the substrate. The figure shows that the top of the batt and attic air temperatures were both higher than the bottom of the batt temperature for the heating portion of the day (≈550 min. - 1200 min.). This indicates that during the heating portion of the day the temperature gradient was such that heat would be transferred into the house. Due to paper length constraints, this figure serves as a typical representation of temperature-time histories while data for other days have been collected and are similar in behavior.

Figure 4 shows the measured relative humidity at the top and bottom of the R-30 insulation batts for both with and without a plastic vapor barrier at the substrate. The relative humidities at the top of the batt for both cases are essentially the same. The top of the batt relative humidities are higher during the early morning (≈0 min. - 450 min.) and decreases rapidly during the heating portion of the day as expected. However, in comparing the bottom of the batt relative humidities for the two batts it can be seen that the batt with a plastic vapor barrier has a significantly higher measured relative humidity than the batt without a vapor barrier. Using the dry bulb measured temperatures and relative humidities from Figs. 3 and 4, respectively, the calculated dimensionless vapor H_2O concentrations are presented in Fig. 5. Shown in Fig. 5 are the calculated dimensionless vapor H_20 concentration histories for batts both with and without a vapor barrier. The insulation batt without a vapor barrier shows that the vapor concentration at the top of the batt

is always greater than that at the substrate; hence for this batt there is always a gradient between the top and bottom of the batt such that there will be a diffusion of vapor H_2O from the top of the batt to the bottom. For the batt with a plastic vapor barrier, the H_2O vapor concentration gradient between the top and bottom of the batt at any given time is quite small; hence diffusion of vapor H_2O within this insulation batt is significantly decreased with the implementation of the plastic vapor barrier. With the above temperature profiles (Fig. 3) and concentration profiles (Fig. 5) employed as boundary conditions, the predicted and measured heat fluxes for batts both with and without a plastic vapor barrier are compared in Fig. 6. This figure shows that there is good agreement between the numerical/analytical model and the experimental data. In comparing the batt with a plastic vapor barrier to that without a barrier, it is seen that the heat flux at the substrate has been reduced for the plastic vapor barrier case. Furthermore, Table 2 shows the integrated values for both batts and it is shown that the time-integrated substrate heat flux is reduced by 14% (comparing the experimental data) during the heating portion of the day with the utilization of a plastic vapor barrier (while the numerical model showed a reduction of 12% during the heating portion of the day) .

Figure 7 demonstrates the additional usefulness of the numerical/analytical model, that is, with this model the three modes of heat transfer can be individually analyzed. Figure 7 depicts how the three different modes of heat transfer (conduction, radiation, and H_2O vapor diffusion) at the substrate are affected once a plastic vapor barrier is in place. The moisture transport mode of heat transfer due to vapor H_2O diffusion was reduced over the entire 24-hour period when a plastic vapor barrier is used. With the plastic vapor barrier in place, the H_2O vapor is not permitted to diffuse through the substrate and into the living space but is absorbed or desorbed throughout the entire batt. Note also that there is a non-negligible amount of moisture which is

absorbed and desorbed near the substrate within the fiberglass insulation phenolic binder. Near the substrate, the phenolic binder acts as an desiccate and absorbs or desorbs the vapor H_2O. Therefore, Fig. 7 shows that even with a plastic vapor barrier at the substrate, a vapor H_2O diffusion gradient exists near the substrate which is associated with H_2O absorption and desorption into and out of the phenolic binder and not mass diffusion through the plastic barrier. The conduction and radiation modes are only reduced slightly once a plastic vapor barrier is incorporated. This is because once a vapor barrier is used the mass transfer is reduced and hence the energy associated with the mass transfer is reduced, therefore changing the temperature field near the substrate which slightly decreases the conduction and radiation modes of heat transfer. Figure 8 displays dimesionless spatial vapor H_2O concentration profiles at different times of the 24-hour period for both batts. For each of these time instances the batt with a plastic vapor barrier has a lower vapor H_2O concentration gradient at the substrate while the profile of the batt without a plastic vapor barrier shows that the absolute concentration is lower at the bottom of the batt and increases linearly towards the top of the batt. Figure 7 shows that all three modes of heat transfer were reduced with the addition of a plastic vapor barrier and Fig. 8 illustrated that the vapor H_2O concentration profiles become more uniform once a plastic vapor barrier had been added. Combining the results of these two figures explains why the overall substrate heat flux levels are reduced in Fig. 6 with the implementation of a plastic vapor barrier. Table 2 shows the time-integrated heat flux for the batts with and without a plastic vapor barrier. It can be seen that the time-integrated heat flux was reduced by 14% for the experimental data and 12% for the theoretical model when comparing a standard R-30 batt with a plastic vapor barrier batt. In Table 2 the experimental data and the numerical model show very good agreement for the standard R-30 batt and the R-30 batt with a plastic vapor barrier at the substrate, 4.7% and 2.5% respectively.

Radiant Barrier Substrate

Figure 9 depicts the overall predicted substrate heat flux-time histories for the non-perforated radiant barrier batt compared to the predicted heat flux-time histories for the plastic vapor barrier batt from Fig. 6 and also shown is the measured plastic vapor barrier data from Fig. 6. All three sets of results show close agreement which implies that the non-perforated foil radiant barrier does yield basically the same results as a plastic vapor barrier. The predicted heat flux level at the substrate did not significantly change (less than 1%) when a non-perforated foil radiant barrier was used as compared to the plastic vapor barrier. Again the usefulness of the numerical/analytical model shows that even though the heat flux at the substrate did not significantly change in Fig. 9, it can be seen in Fig. 10 that there was a change in the three modes of heat transfer at the substrate. From Fig. 10 it can be seen that the radiation mode of heat transfer at the substrate is practically eliminated once a non-perforated foil radiant barrier is added at the substrate however this is only true at the substrate there is still significant amount of radiation through out the insulation batt (the reader is once again reminded that the non-perforated foil radiant barrier is assumed to act as a non-perforated vapor barrier therefore the comparisons in Fig. 10 are those of a predicted non-perforated radiant barrier case and no radiant barrier at the substrate case). The radiant energy that was associated with the radiation mode of heat transfer for the plastic vapor barrier case is now (non-perforated radiant barrier) reflected from the substrate back into the insulation batt where this energy is absorbed near the substrate and increases the temperature gradient at the substrate and hence causes an increase in the conduction mode of the heat transfer. The conduction mode for the non-perforated radiant barrier substrate was increased by about the same amount that the radiation mode was decreased when compared to the plastic vapor barrier case. The heat transport due to H_2O transport was not significantly

affected by this predicted implementation of a non-perforated foil radiant barrier as compared to the plastic vapor barrier. The net effect is that there is essentially no change in the overall substrate heat flux level, but the radiation and conduction modes are strongly altered. Table 2 shows that the numerical model time-integrated heat flux was changed by about 1% when comparing a non-perforated foil radiant barrier substrate batt to a batt with a plastic vapor barrier at the substrate. Figure 11 depicts a comparison between the predicted perforated radiant barrier batt and that of the measured and predicted no vapor barrier batt (Fig. 6). Over the entire 24-hour period there is no significant difference between the three sets of results. The substrate heat flux for the predicted cases of either a perforated foil radiant barrier or no vapor barrier are practically identical. There was essentially no change in the predicted substrate heat flux; however, in Fig. 12 it can be seen that the radiation mode was strongly reduced for the perforated radiant barrier case when compared to the case without any substrate barrier. This nullification of the radiation mode causes an increase in the conduction mode because the radiant energy is reflected back into the insulation batt and is absorbed by the fiberglass and then is changed into conduction heat transfer as explained earlier (Fig. 10). As shown in Fig. 12, the conduction mode of heat transfer increased considerably with the addition of a perforated foil radiant barrier at the substrate. The vapor H_2O diffusion mode of heat transfer did not change for the case with a perforated radiant barrier as compared to the case with no substrate barrier. Since the vapor H_2O diffusion mode did not change and the changes in the conduction and radiation modes offset one another, the overall heat transfer at the substrate did not change significantly with the use of a perforated radiant barrier as compared to a case with no substrate barrier. Table 2 shows that the "model" integrated heat transfer was only altered by 2% when comparing a standard R-30 insulation batt to a batt with a perforated radiant barrier substrate.

Vapor Barrier at Substrate and Radiant Foil Barrier Above

Previous works [3-4] showed that the time-integrated substrate heat flux can be reduced as much as 27% once a foil radiant barrier is placed "above" a R-30 fiberglass insulation batt. Thus far, this investigation showed that the time-integrated substrate heat flux can be reduced by 14% (Table 2) once a plastic vapor barrier is applied to the substrate of a R-30 fiberglass insulation batt. It would appear that a combination of these two barriers (plastic below and foil above) would yield a time-integrated substrate heat flux reduction of approximately 41% (14% and 27%). Figure 13 illustrates the results on the substrate heat flux for June 25, 1994 when the combination of a plastic vapor barrier at the substrate and a foil radiant barrier above the R-30 batt are employed. This combination is compared to an insulation batt without a substrate barrier and no radiant barrier above (i.e. standard R-30 batt). The time-integrated heat flux levels over the heating portion of the day are tabulated in Table 2, the experimental time-integrated measured heat flux at the substrate is reduced by 37% when compared to the standard insulation batt.

CONCLUSIONS

This paper has presented an investigation of the changes in the substrate heat flux levels and the changes in the different modes of heat transfer (conduction, radiation and moisture transport) when a plastic vapor barrier, a non-perforated foil radiant barrier, or a perforated foil radiant barrier was implemented at the substrate of a R-30 fiberglass insulation batt. The addition of a plastic vapor barrier at the substrate reduced the substrate time-integrated heat flux by 14% when compared to a no substrate barrier case (standard R-30 batt). It is significant to realize that a 14% (based on the measured data) decrease in the time-integrated substrate heat flux through the ceiling into a home during the summer season can help the overall national energy savings and pollution reduction. With the addition of either a perforated or a non-perforated radiant barrier

at the substrate the heat flux essentially did not change when compared to the no substrate radiant barrier and plastic vapor barrier cases, respectively. As demonstrated, the use of a radiant barrier substrate will have essentially no effect (less than 2%); however, as discussed in the results section, the different modes of heat transfer were strongly affected when substrate radiant barriers were applied. The use of a plastic vapor barrier was also found to reduce the time-integrated substrate heat flux levels by 14% (Table 2) into the living area of a residential home as compared to the case of a standard R-30 fiberglass batt without any substrate barrier; in a previous work [1] for R-19 this reduction was 13%.

It should be noted that only representative data have been shown for all of the cases above; however numerous days of data were obtained for all of the experimental conditions. The experimental data confirm the results presented in this paper over a time period of many weeks. Further, this paper investigated the results of combining a plastic vapor barrier at the substrate with a foil radiant barrier above the fiberglass insulation. This combination resulted in a time-integrated substrate heat flux reduction of 37% (based on the measured data) when compared to a standard R-30 insulation batt. A 37% reduction in the time-integrated substrate heat flux through the ceiling into the home can yield a considerable savings in energy consumption; in a previous work [1] for R-19 the reduction was 52% for such a combination configuration.

REFERENCES

[1] Harris,K.T., McCarty,T.A., Roux,J.A., "Substrate Barrier Effects for a R-19 Fibrous Insulation Batt", The Journal of Thermal Insulation and Building Envelopes, Vol. 19, July 1995, pp. 28-48.

[2] Levins, W.P., Karnitz, M.A., and Hall, J.A., "Moisture Measurements in Single-Family

Houses with Attics Containing Radiant Barriers", Oak Ridge National Laboratory, Report ORNL/CON-255, February 1989.

[3] Gorthala, R., Roux, J. A. and Fairey III, P. W.,"Combined Conduction, Radiation Heat Transfer and Mass Transfer in Fibrous Attic Insulations," Insulation Materials: Testing and Applications, 2nd Volume, ASTM STP 111, American Society for Testing and Materials, Philadelphia, 1991, pp. 371-386.

[4] Harris, K.T., McCarty, T.A., Roux, J.A., and Gorthala, R., "Total Heat Transfer Due to the Variation in Fiberglass Insulation Thickness in Attics," ASME National Conference on Heat Transfer, August 8-11, Radiative Heat Transfer Theory and Applications, HTD-Vol. 244, 1993, pp. 1-10.

[5] Gorthala, R., Harris, K.T., Roux, J.A., and McCarty, T.A., "Transient, Conductive, Radiative Heat Transfer Coupled with Moisture Transport in Attic Insulations," Journal of Thermophysics and Heat Transfer, Vol. 8, No. 1, Jan.-Mar. 1994, pp. 125-132.

[6] Yarbough, D., Personal Communication, Oak Ridge National Laboratory, March 1994.

[7] Wilks, K., Personal Communication, Oak Ridge National Laboratory, June 1994.

[8] Fairey, P., Personal Communication, Florida Solar Energy Center, June 1994.

[9] Hust, J. G., Callanan, J. E., and Sullivan, S. A.,"Specific Heat of Insulations," Thermal Conductivity 19, D. W., Yarbrough, Ed., Plenum, N.Y., 1988, pp. 533-550.

[10] Yeh, H. Y., and Roux, J. A., "Spectral Radiative Properties of Fiberglass Insulation", Journal of Thermophysics and Heat Transfer, Vol. 2, No. 1, January 1988, pp. 75-81.

[11] Patankar, S. V., Numerical Heat Transfer and Fluid Flow, Hemisphere Publishing Corp., Washington, D.C., 1980.

[12] Hansen, K. K.,"Sorption Isotherms," A Catalogue, Building Materials Laboratory,

Department of Civil Engineering, The Technical University of Denmark, 1985.

[13] Tchernev, D.I., "Exploration of Molecular Sieve Zelolites for the Cooling of Buildings with Solar Energy," Report: NSF/RA - 770017.

[14] Tchernev, D.I.,"Solar Energy Application of Natural Zeolites," Natural Zeolite and Its Use, Oxford, New York, Pergamon Press, 1978, pp. 479-484.

[15] Langlais, C., Hyrien, C., Klarsfeld, S., "Moisture Migration in Fibrous Insulating Materials under the Influence of a Thermal Gradient and Its Effect on Thermal Resistance," Moisture Migration in Buildings, ASTM STP 779, 1982, pp. 191-206.

[16] Roux, J. A., Smith, A. M., and Todd, D. C., "Radiative Transfer with Anisotropic Scattering and Arbitrary Temperature for Plane Geometry," AIAA Journal, Vol. 13, No. 9, Sept. 1975, pp.1203-1211.

[17] Rish, J.W. and Roux, J.A., "Heat Transfer Analysis of Fibrous Insulations With and Without Radiant Barriers for Summer Conditions," Journal of Thermophysics and Heat Transfer, Vol.1 No.1, 1987, pp.43-49.

[18] Houston, R.L. and S.A. Korpela, "Heat Transfer Through Fiberglass Insulation", Proceeding of the 7th International Heat Transfer Conference, Vol. 2, 1982, pp.449-504.

[19] Yajinik, S., J.A. Roux, " Determination of Radiative Properties of Fiberglass and Foam Insulation," Report ORNL/Sub/86-55930/1, 1986 Oak Ridge National Laboratory.

[20] Holman, J.P., 1990, Heat Transfer, 7th Ed. McGraw-Hill Publishing.

[21] Tao, Y.X., R.W. Besant and K.S. Rezkallah, "Transient Thermal Response of a Glass-Fiber Insulation Slab with Hygroscopic Effects", International Journal of Heat and Mass Transfer, Vol. 35, No. 5, May 1992, pp.1155-1167.

TABLE 1. Radiative and thermal properties used in numerical computations.

ρ_f[a]	12.0	kg/m^3
c_f[a]	844.4	J/kg-K
k_f[b]	$a + bT + 8.5537 \times 10^{-5} \rho_f$	W/m-K
	$a = 4.97576 \times 10^{-3}$, $b = 7.00025 \times 10^{-5}$	
ω[c]	0.201	
β[c]	3.70	cm^{-1}
γ_{vR}[d]	1.2×10^{-5}	m^2/s
γ_b[e]	1.19×10^{-9}	m^2/s
m_ϕ[f]	$1/100 \quad .10 \leq \phi \leq .90$	
γ_v/γ_{vR}[d]	$(T/T_R)^{1.5}$	

[a]Ref.[9], [b]Ref.[18], [c]Ref.[19], [d]Ref.[20], [e]Ref.[21], [f]Ref.[11]

subscript R represents referenced values.

TABLE 2. Time integrated substrate heat flux levels corresponding to R-30 fiberglass batt with a plastic vapor barrier or non-perforated foil radiant barrier or a perforated foil radiant barrier for summer conditions.

Date Configuration		Case	Heating[a] Portion R-30 kJ/m^2	Reduction	Comparison
7/27/94 Standard R-30 Batt		Model	-30.4		
		Data	-31.9		(4.7%)[f]
7/27/94 Plastic Vapor Barrier		Model	-26.6	[12%][b]	
		Data	-27.3	[14%][b]	(2.5%)[f]
7/27/94 Substrate Radiant Barrier	Non-perforated	Model	-26.9	([1%])[c]	
	Perforated	Model	-29.8	([2%])[d]	
6/25/94 Plastic Vapor Barrier Below and Radiant Barrier Above		Model	-19.1	{37%}[e]	
		Data	-20.2	{37%}[e]	(5.4%)[f]

[a]Integrated over heat gain period (550 min < t < 1210 min).
[b]Reduction in substrate heat flux when comparing plastic vapor barrier case with standard R-30 batt.
[c]Change in substrate heat flux when comparing non-perforated radiant barrier substrate case with plastic vapor barrier case (model only).
[d]Change in substrate heat flux when comparing perforated radiant barrier case with standard R-30 batt (model only).
[e]Reduction in substrate heat flux when comparing a batt with a plastic vapor barrier below and a radiant barrier above with a standard R-30 batt (data or model).
[f]Comparison of model and data for a given configuration.

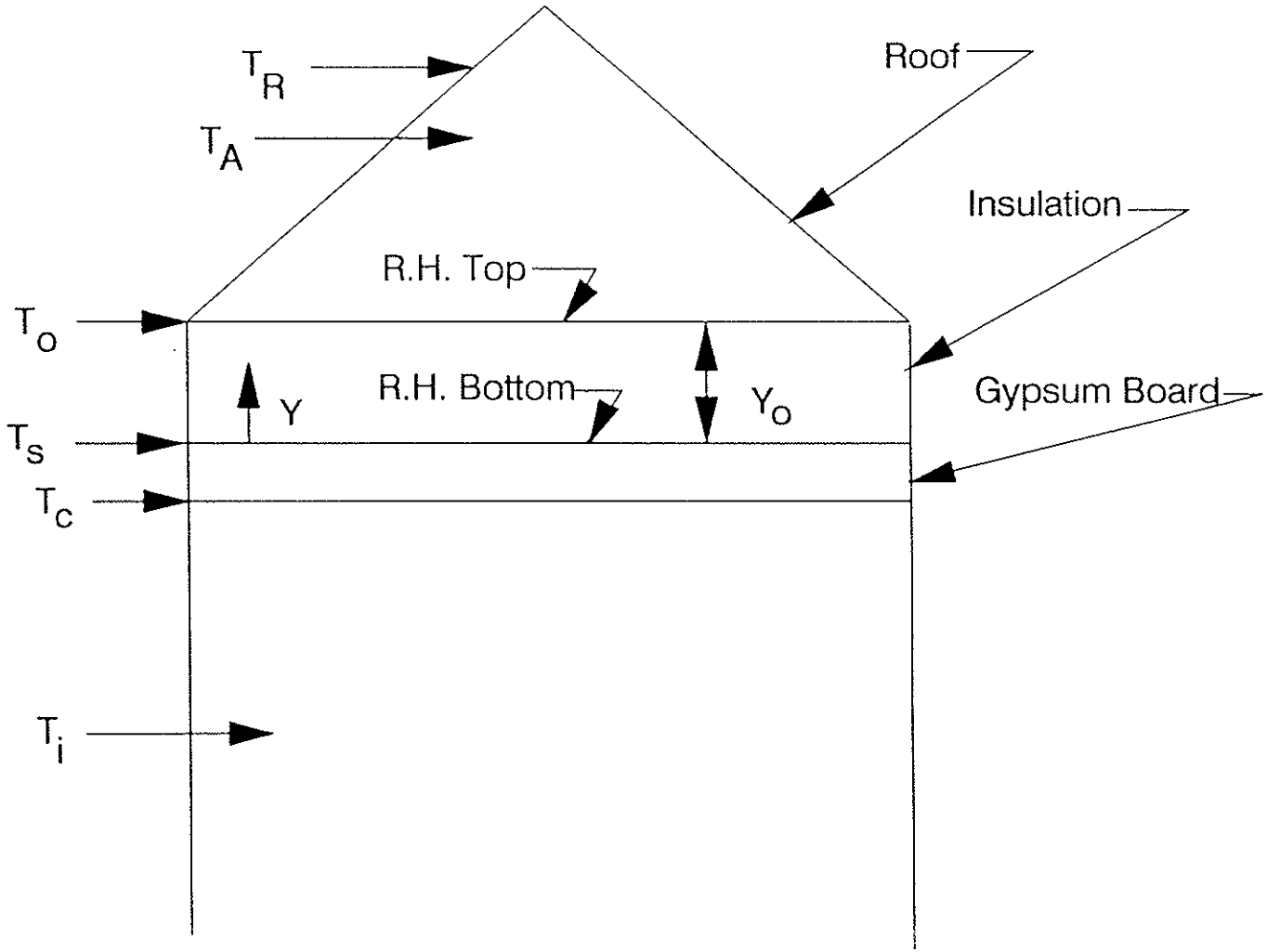

Fig. 1 Attic sketch.

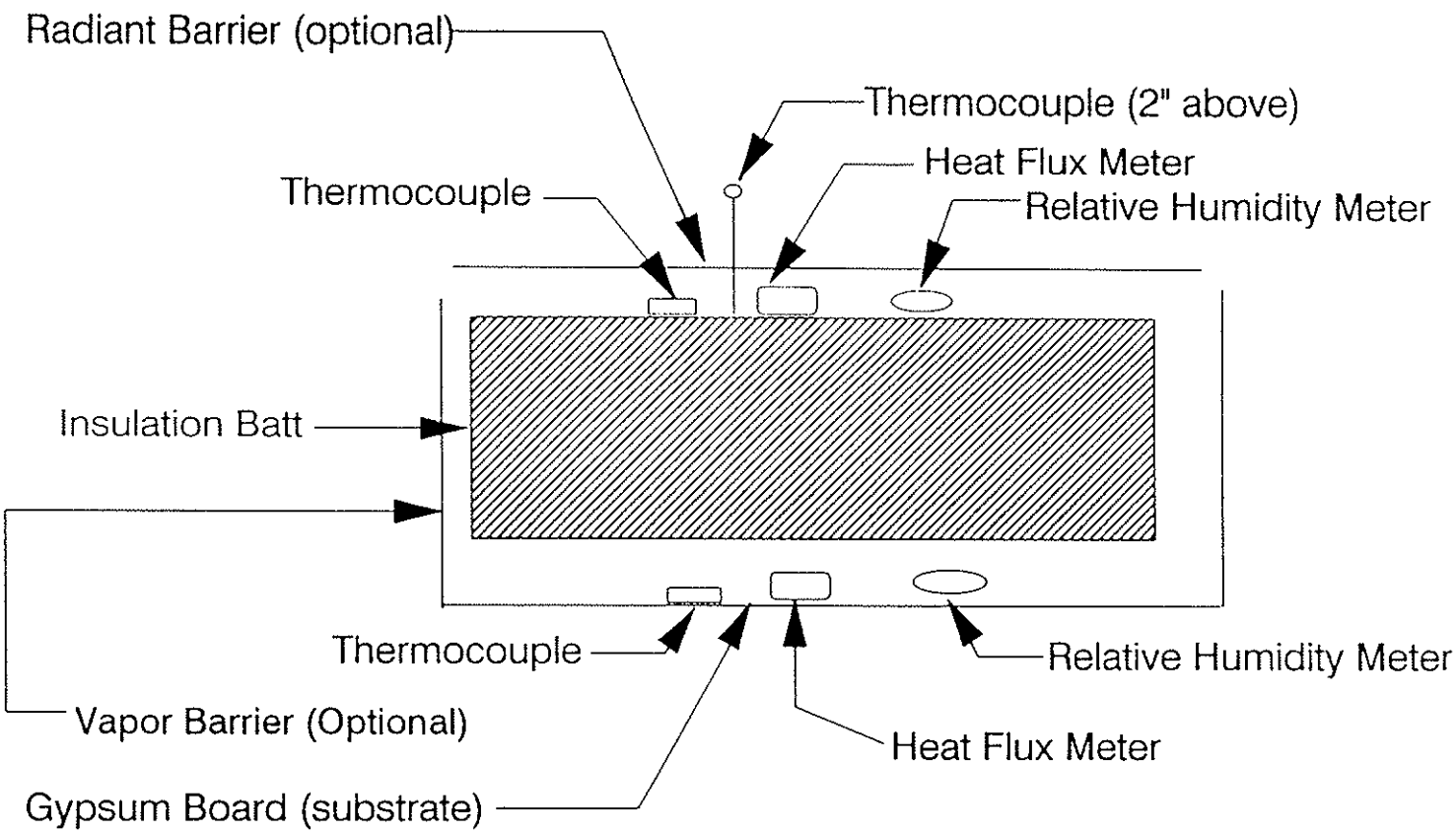

Fig. 2 Location of heat flux meters, relative humidity meters and thermocouples about the insulation batt.

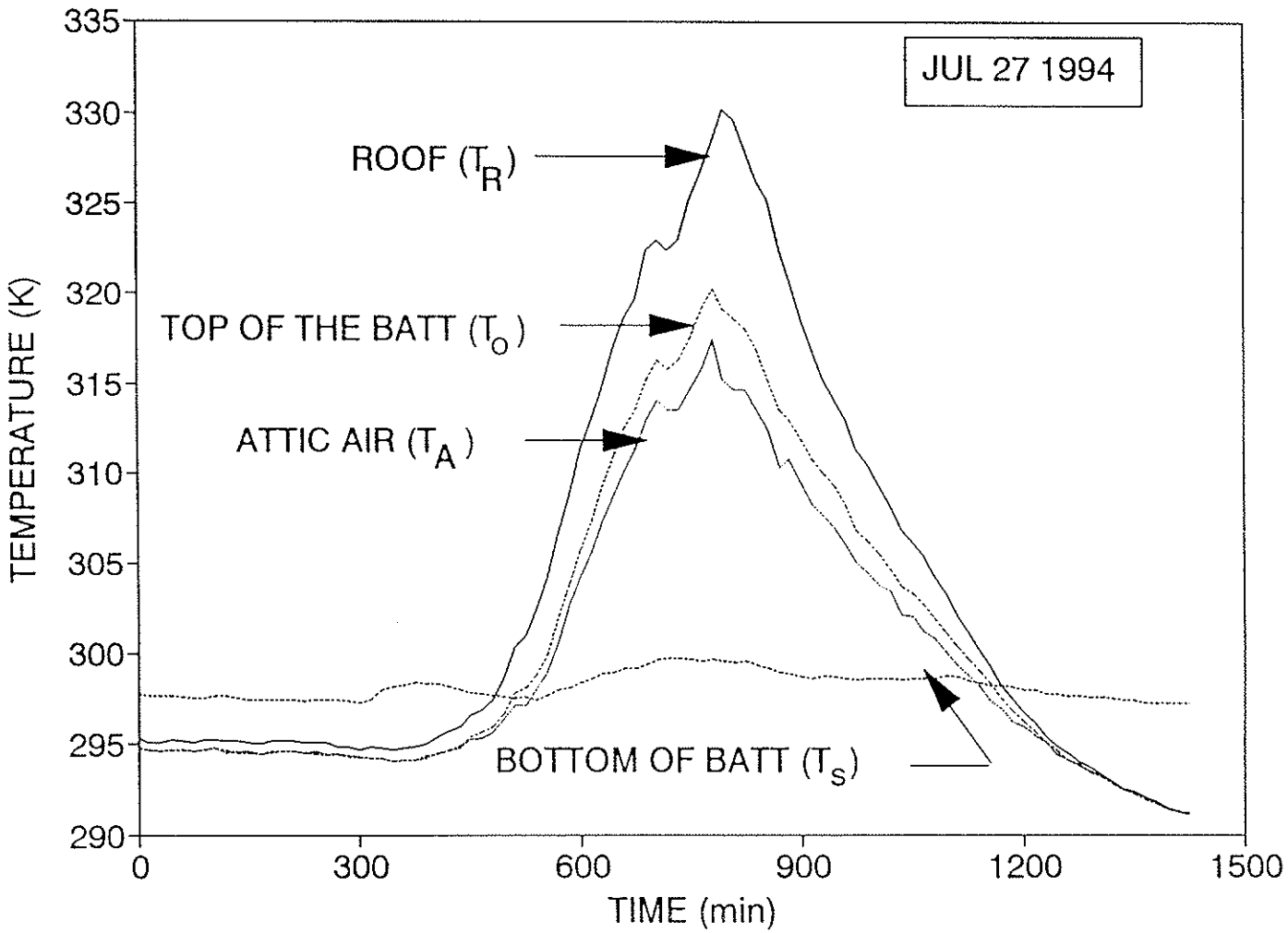

FIGURE 3. Temperature-time histories for a R-30 fiberglass insulation batt with a plastic vapor barrier at the substrate.

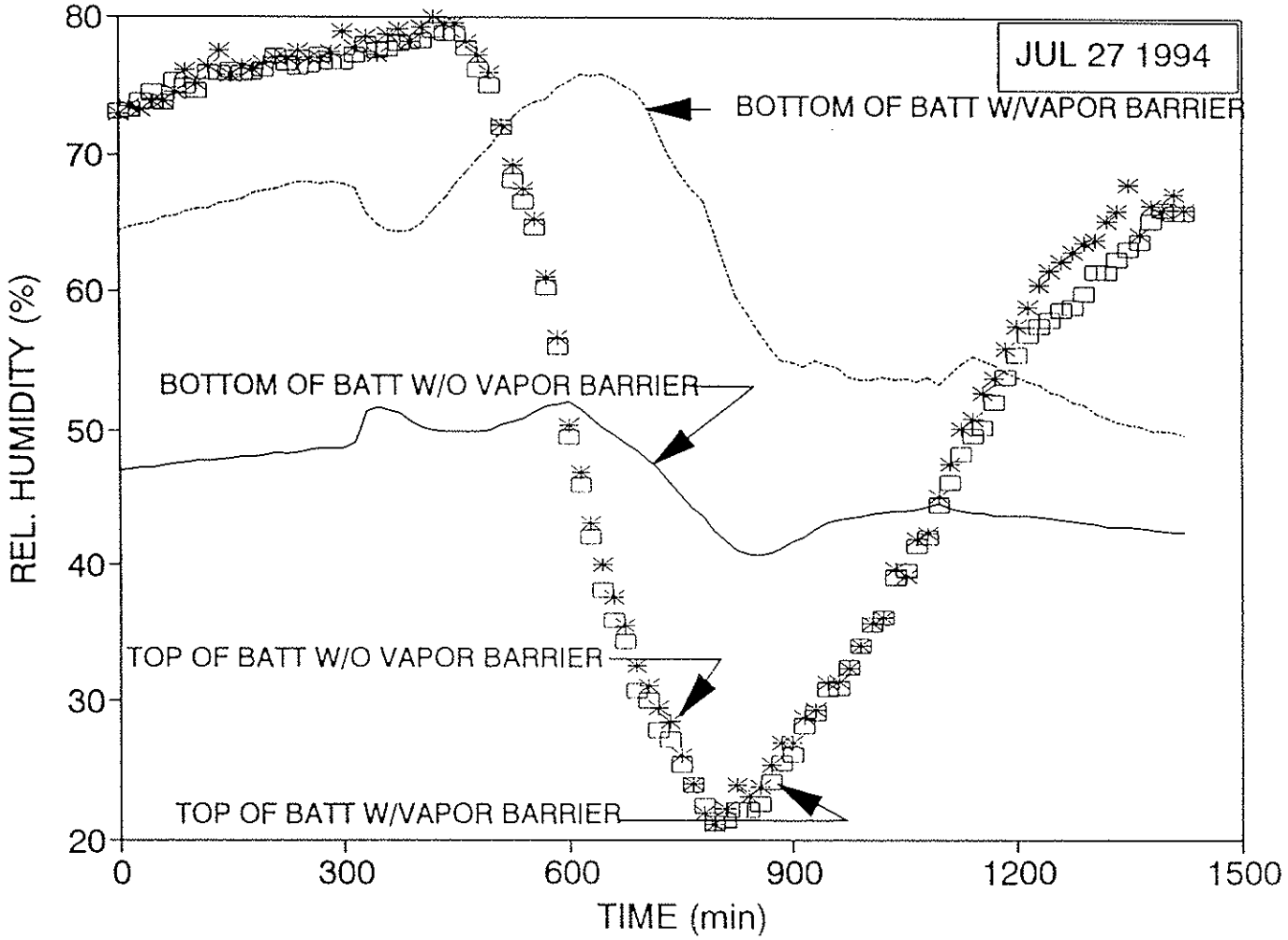

FIGURE 4. Measured relative humidities at different locations of the insulation for both batts with and without a plastic vapor barrier.

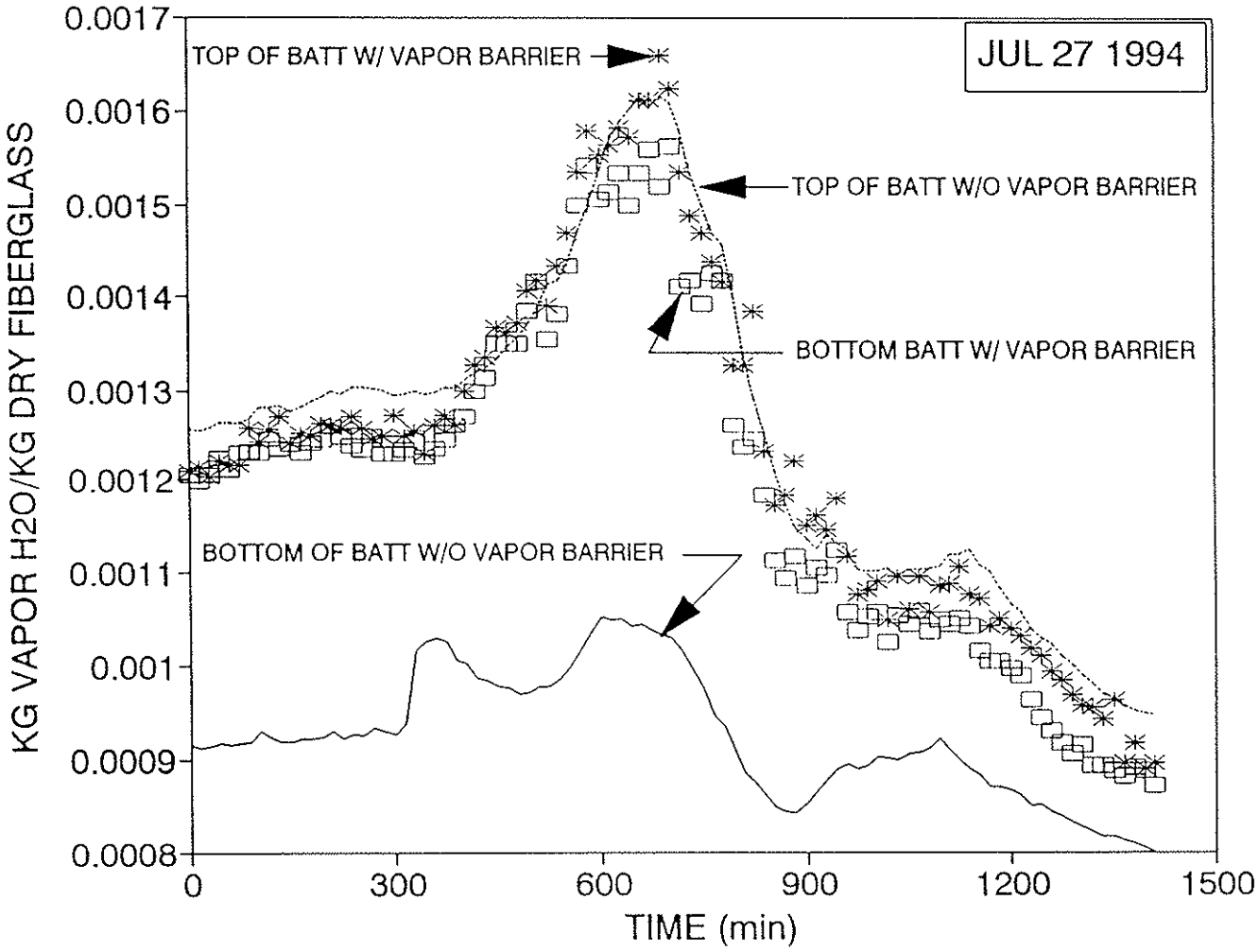

FIGURE 5. Vapor H2O concentration histories for both batts with and without a plastic vapor barrier at the insulation substrate.

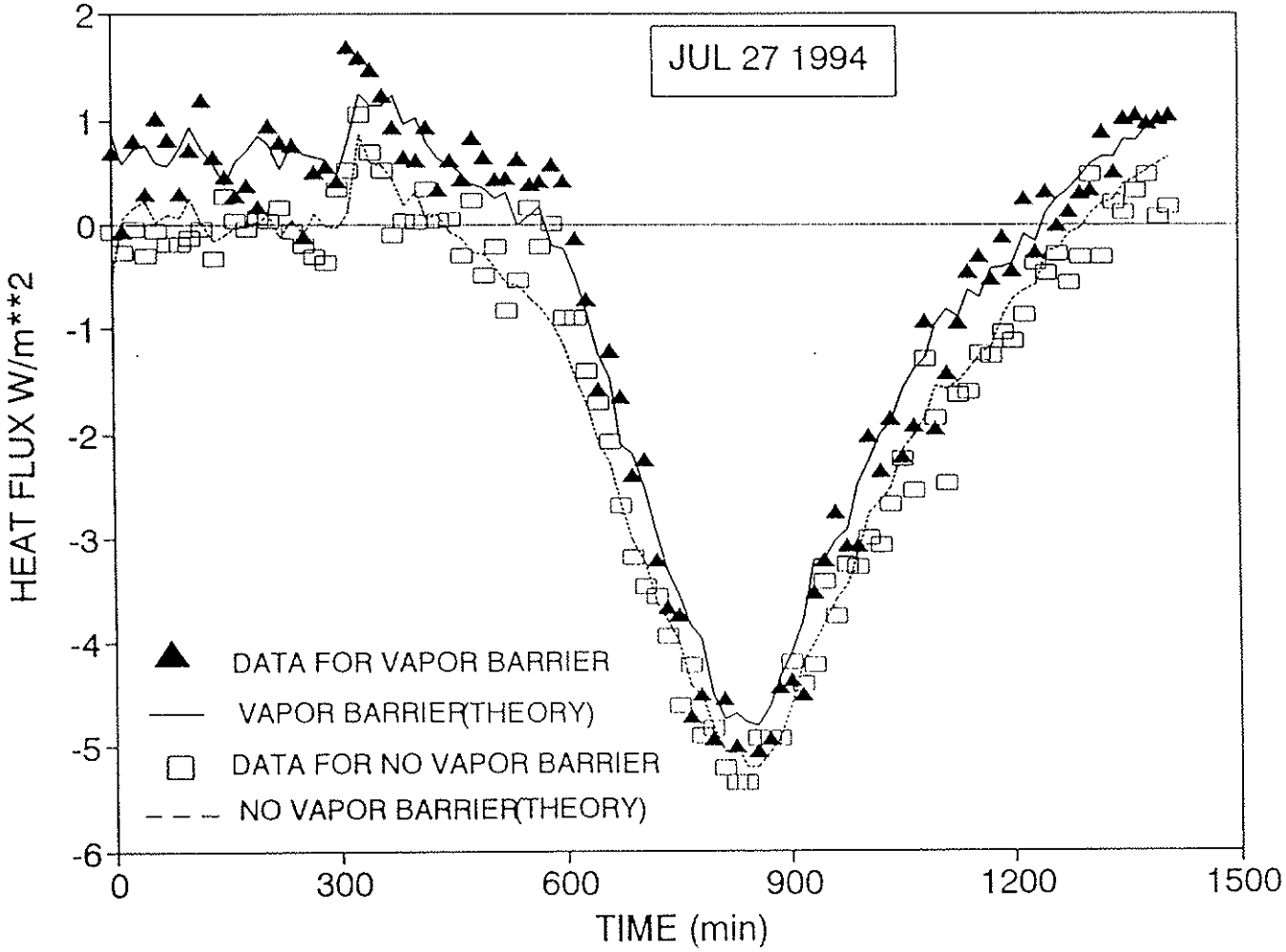

FIGURE 6. Substrate measured and predicted heat flux-time histories for both cases with and without a plastic vapor barrier.

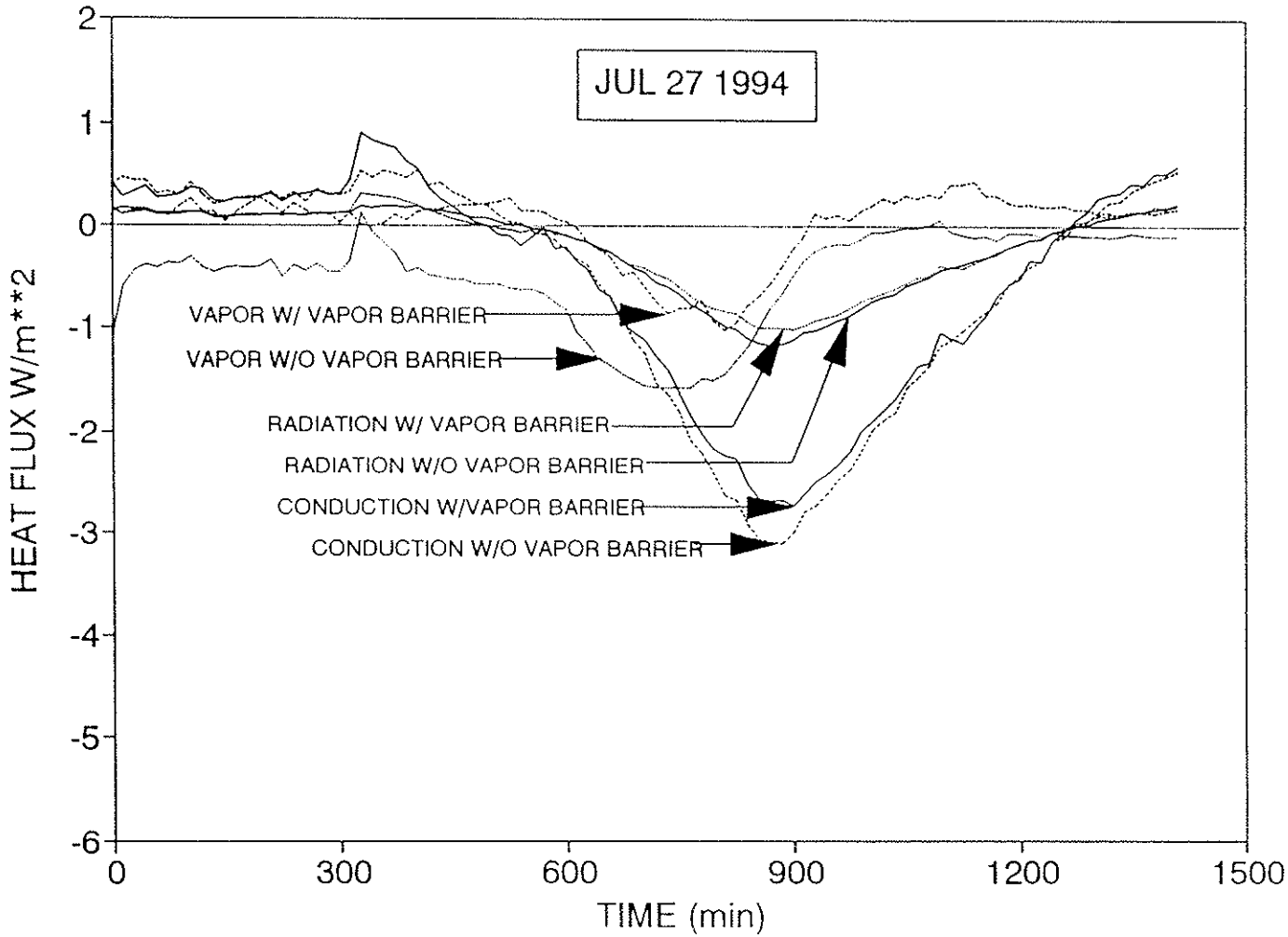

FIGURE 7. Predicted substrate heat flux-time histories for the conduction, radiation, and vapor H2O heat transfer modes.

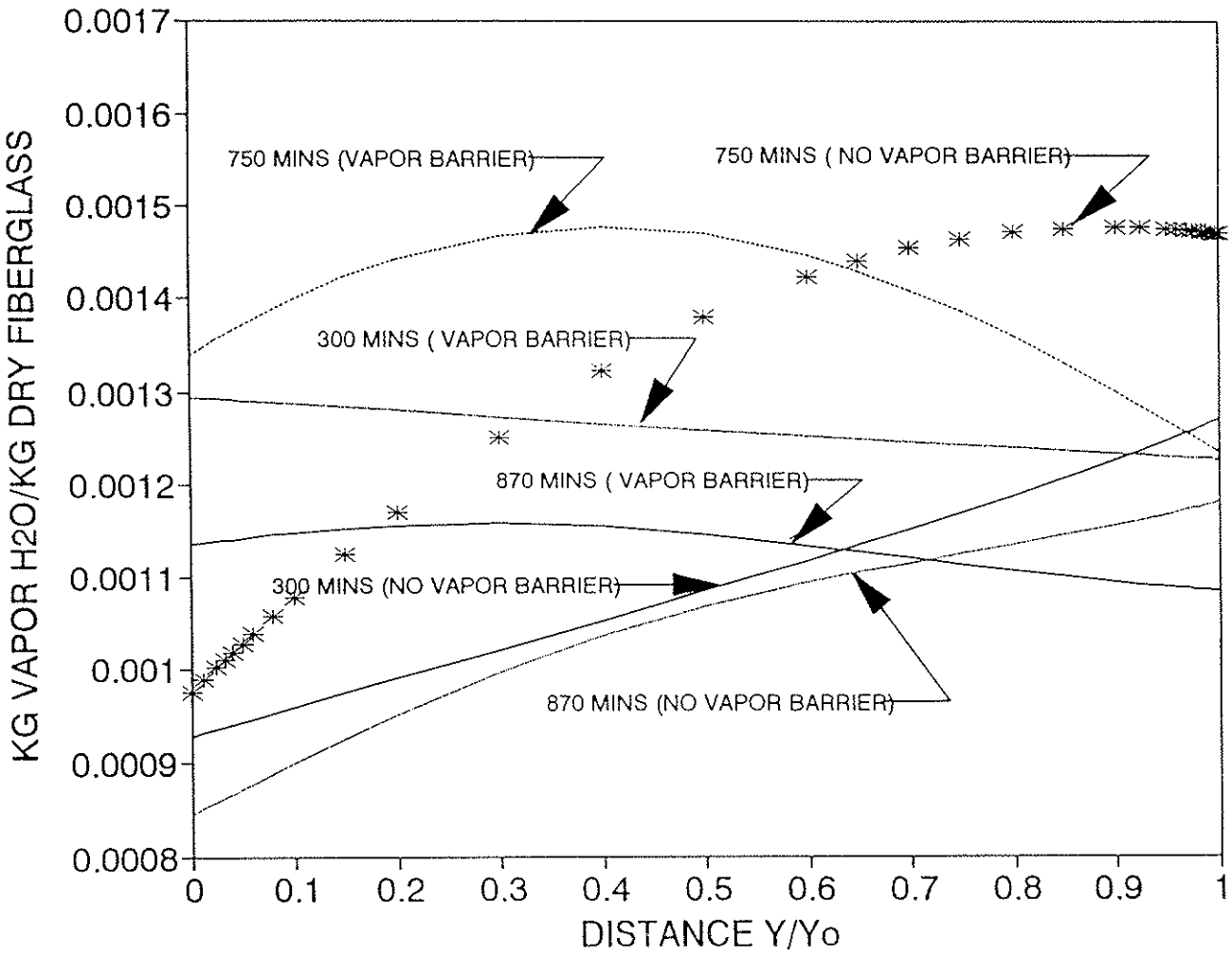

FIGURE 8. Spatial concentration profiles for different time instances for R-30 insulation with and without a plastic vapor barrier.

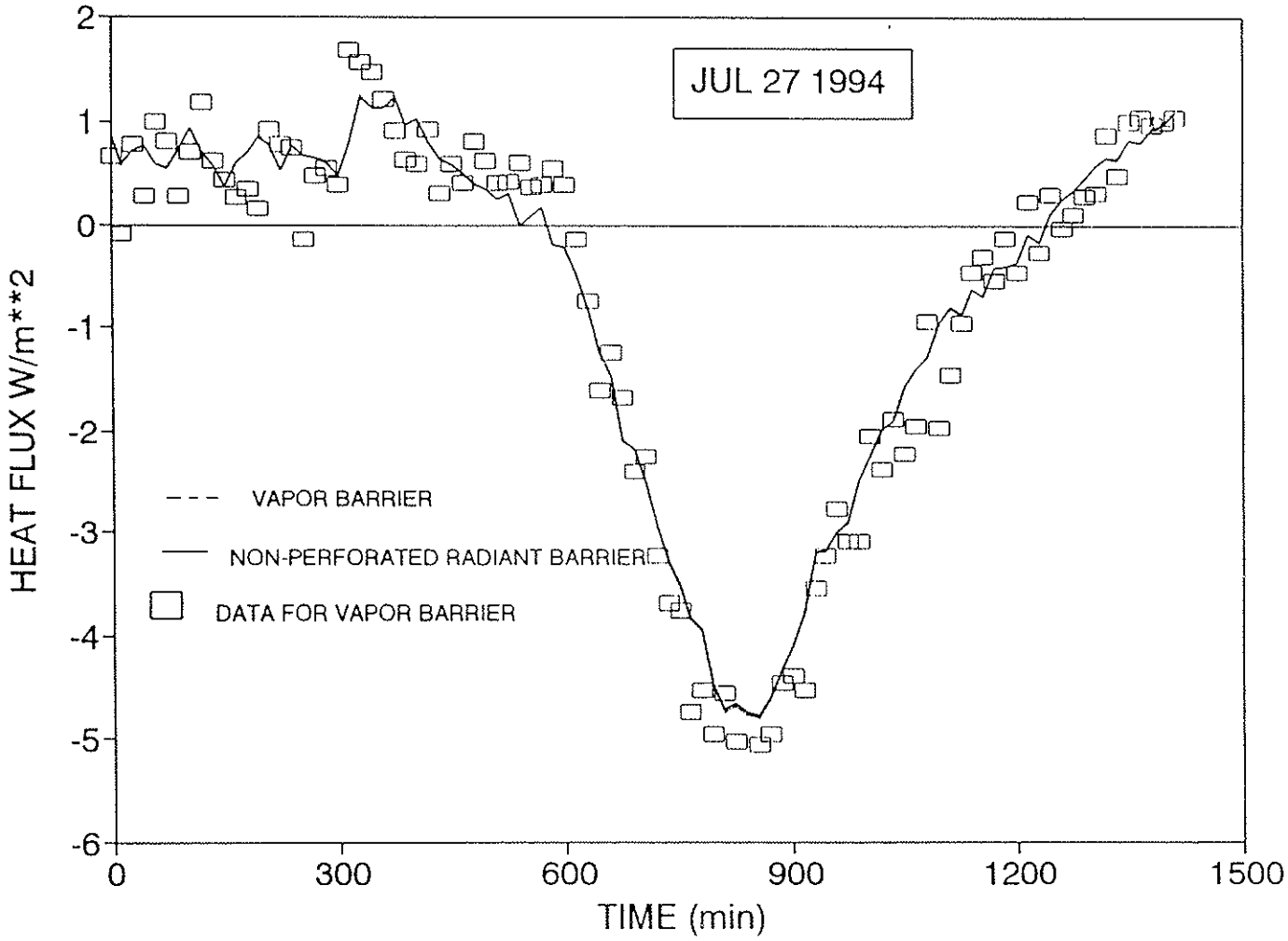

FIGURE 9. Substrate measured and predicted heat flux -time histories for both with and without a non-perforated radiant barrier.

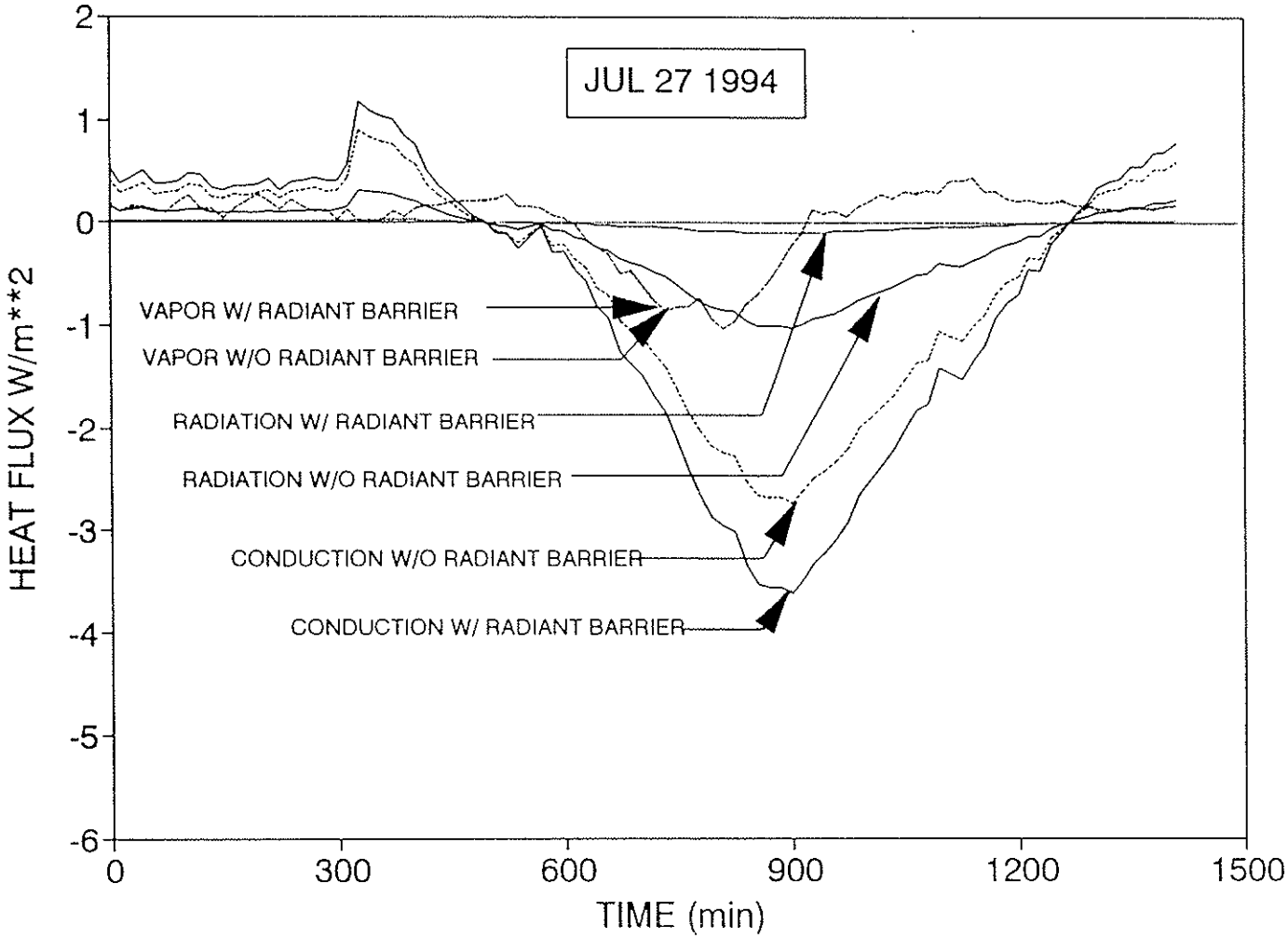

FIGURE 10. Predicted substrate heat flux-time histories for the conduction, radiation, and vapor H2O diffusion modes for a batt with and without a non-perforated radiant barrier.

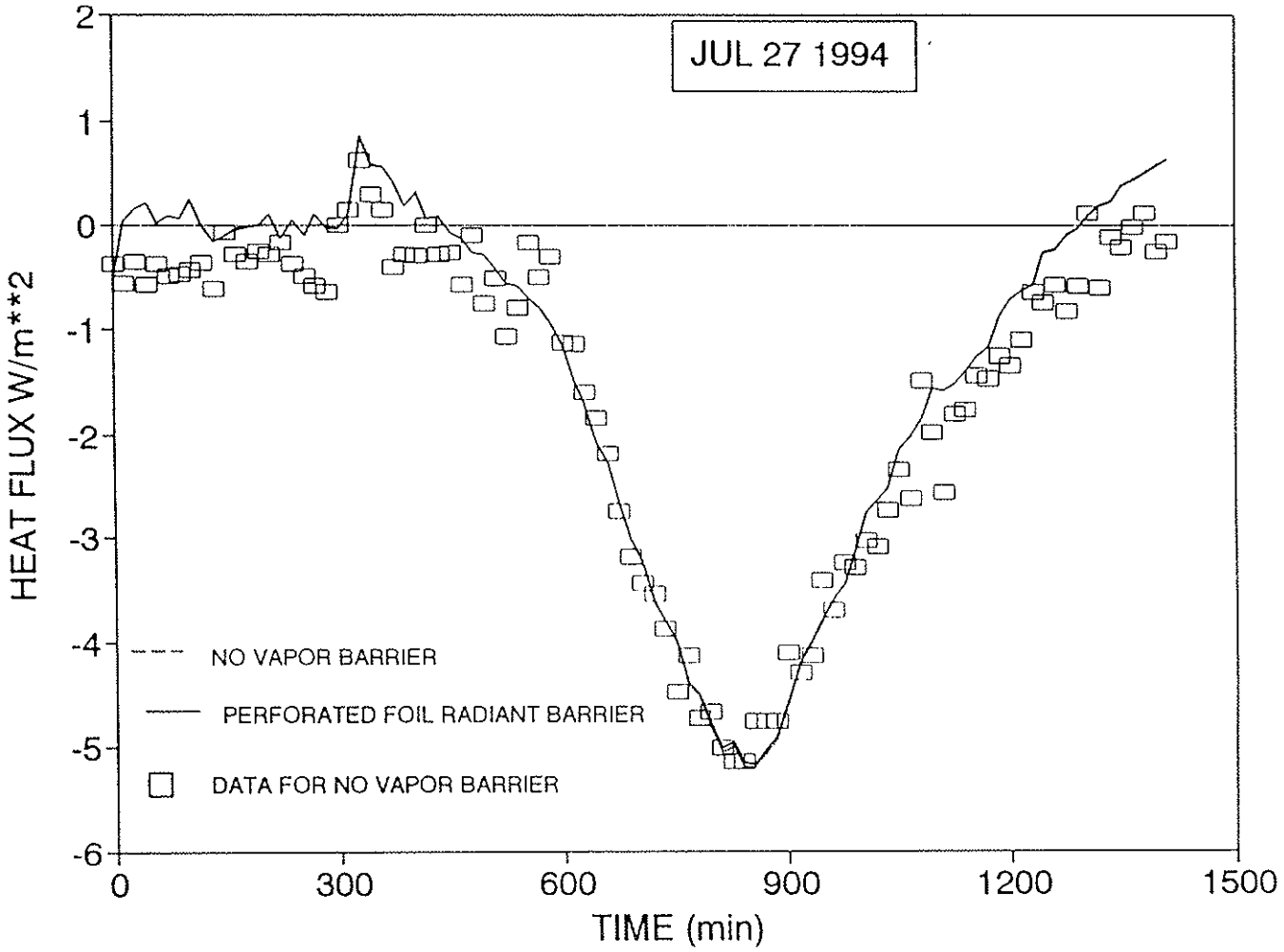

FIGURE 11. Substrate measured and predicted heat flux-time histories for both with and without perforated radiant barrier.

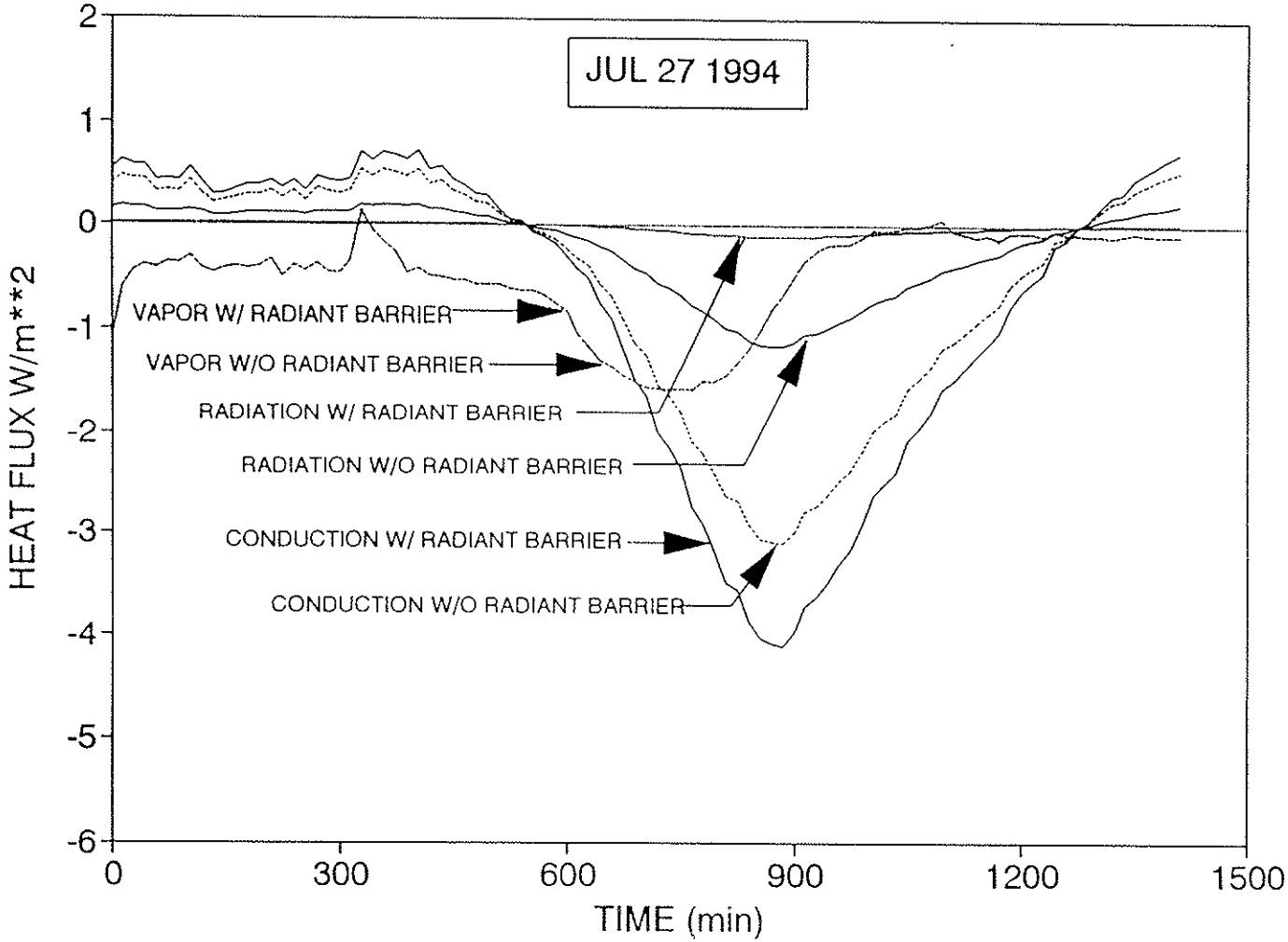

FIGURE 12. Predicted substrate heat flux-time histories for the conduction, radiation, and H2O vapor diffusion modes for a batt with and without a perforated radiant barrier.

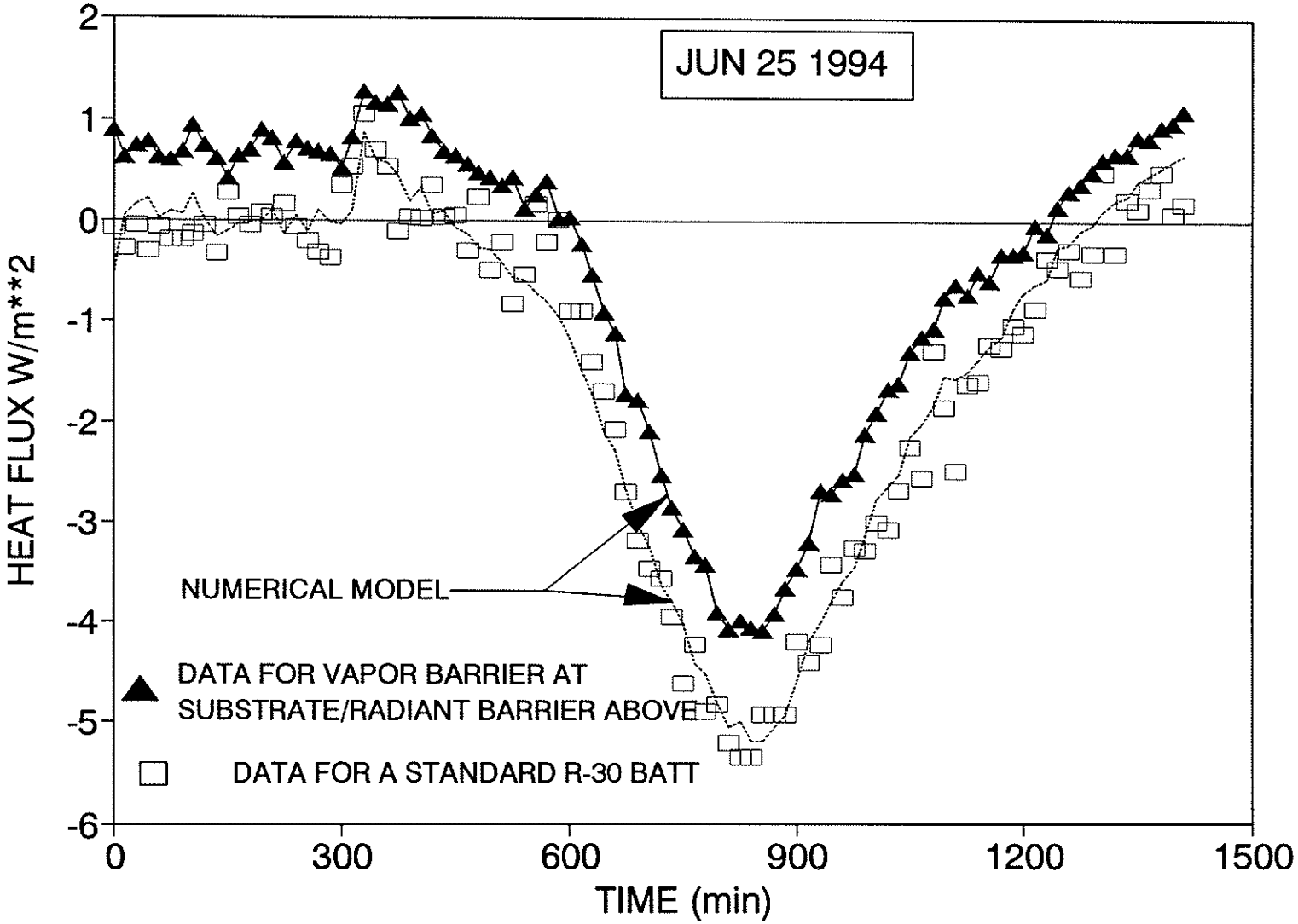

Figure 13. Substrate measured and predicted heat flux histories for a batt with a plastic vapor barrier at the substrate and a foil radiant barrier above as compared to a standard R-30 insulation batt.